Chemical Engineering Research and Design 208 (2024) 683–694

Contents lists available at ScienceDirect

Chemical Engineering Research and Design

journal homepage: www.elsevier.com/locate/cherd

Experimental and numerical investigation of an innovative desalination unit under laminar, transient, and turbulent flow conditions

Faizan Ahmed [a,b], Mohd Sharizal Abdul Aziz [a,*], Feroz Shaik [b], C.Y. Khor [c]

[a] School of Mechanical Engineering, Engineering Campus, Universiti Sains Malaysia, Nibong Tebal, Seberang Perai Selatan, Penang 14300, Malaysia
[b] Mechanical Engineering Department, Prince Mohammad Bin Fahd University, Al Khobar, Saudi Arabia
[c] Faculty of Mechanical Engineering & Technology, Universiti Malaysia Perlis (UniMAP), Perlis, Malaysia

ARTICLE INFO

Keywords:
Flow rate
Concentrated solar energy
Desalination system
Efficiency
Energy analysis
Exergy analysis

ABSTRACT

Solar-based desalination systems face problems such as interruptions in the supply of solar energy or insufficient levels of available solar energy due to geographical or weather conditions, which results in a drop in system performance. To overcome this issue, this study proposes a novel concentrating solar-powered flash desalination system with pressure modulation. The objective of this research is to investigate the influence of flow rate and perform energy and exergy analyses for the proposed novel device. The feed flow rate varied in the range of 0.2–1 L/min. The results revealed that the distillate production increases to an optimum as the flow rate is augmented. The highest product water output of 8880 ml/h was observed at a turbulent flow of 0.8 L/min. The brine heater exhibited an average energetic efficiency of 32 %. Additionally, the flash chamber, brine heater, and condenser exhibited average exergy efficiencies of 32.8 %, 4.1 %, and 89.2 %, respectively. The device achieved the lowest energy consumption of 100.8 kWh/m^3, the highest gain output ratio of 15.5, and the highest energy utilization factor of 4.8. The present findings will assist engineers and researchers in analyzing the impact of feed rate on renewable energy-based desalination devices.

1. Introduction

Freshwater scarcity has become a serious concern as the global population continues to grow along with increased industrial and agricultural production. To tackle this global issue, it is imperative to devise efficient water desalination systems. Currently, membrane-type desalination and thermal-type desalination are two primary methods that are being extensively studied for water purification. Recently, many scientists have focused on membrane desalination, which has shown that new membranes can be developed for desalinating water, such as nanofiltration membranes (Dong et al., 2022). Several researchers are exploring methods for coupling and positioning membranes in conjunction with photothermal materials (Ibrahim et al., 2021) in an attempt to optimize these systems. Utilizing thermal energy to desalinate water is another method, with flash distillation being a typical example. Desalination systems employing flashing techniques vaporize a liquid beneath its saturation pressure (Risse et al., 2012). Due to their remarkable evaporation rates, the desalination industry has widely adopted flash desalination systems. Alongside reducing water wastage, flash desalination systems recover significant amounts of feed water. Another advantage of flashing systems is their efficiency, especially when waste heat is used to heat the feed water. These devices contribute significantly to reducing the carbon footprint of the desalination process. Despite the existence of contaminants and chemicals in ocean water, these devices have drawbacks such as scaling and corrosion. Subsequently, there may be some operational issues, which may lead to an increase in maintenance activities. Some techniques, such as filtration and the addition of chemicals, assist in reducing such issues. Researchers are exploring alternative energy sources for these devices since they depend on non-renewable energy sources (Gandhidasan, 2005). Integrating renewable energy sources will contribute to developing sustainable and efficient desalination systems. The most promising option is solar energy, which is plentiful in nature, available year-round, and easy to convert (Ahmed et al., 2022). However, several problems exist when employing renewable energy in desalinating units. These include inconsistent energy supply or low energy availability levels during operation (Chen et al., 2019).

Various initiatives are being taken to tackle the problems that impact the evaporation rate of desalination systems since the evaporation rate directly influences efficiency. One way to address this issue is through

* Corresponding author.
E-mail address: msharizal@usm.my (M.S. Abdul Aziz).

https://doi.org/10.1016/j.cherd.2024.07.043
Received 4 March 2024; Received in revised form 5 July 2024; Accepted 16 July 2024
Available online 17 July 2024

the storage of energy. To this extent, one study explored storing latent heat in flashing-type desalination units and found that this technique increased performance by 94 % (Miyatake et al., 2001). Another similar research investigated energy storage in desalination devices (Lai et al., 2021) and reported a 9 % overall improvement in efficiency. For energy storage, phase-changing material was used, which significantly increased heat-storing capability. Some scientists (Tareemi and Sharshir, 2023) examined multi-staged flashing desalination units and discovered that the hybridization of systems leads to more energy-efficient systems. Other scientists (Barba and Capocelli, 2023) conducted an investigation of a novel process that integrated multi-effect desalination and flashing-type desalination systems. The new arrangement was 27 % more productive than the previous technique. Even though desalination devices continue to be supported by non-renewable energy input, some scholars are investigating the effect of design alterations to the flashing vessels so that there can be more effective heat transfer inside the flash chamber. In this context, the boiling characteristics of water droplets inside the flashing vessel were investigated upon applying a certain degree of vacuum (Gao et al., 2019). Similarly, another study on the effect of vacuum level (Ahmed et al., 2024) in flashing-type desalination systems was performed, and it was observed that the vacuum level positively impacts distillate production. A different investigation was conducted (Ji et al., 2019), during which flashing was performed at high temperatures and pressure. Their findings suggested that the flashing scenario substantially impacted the bubble development and growth process. In one interesting study (Darawsheh et al., 2019), a double-stage renewable energy-based desalinating unit was examined. The scholars reported that a drop in the air pressure by about 19 % inside the flash vessel contributes to a rise in the distillate by around 53 % while lowering the specific energy consumption (SEC) by approximately 35 %. An optimal distillate production ratio of 0.42 was found, corresponding to 0.5 L/min. Similarly, one simulation study (Kaheal et al., 2023) assessed the efficiency of a unique double-tank unit-based desalinating unit functioning with solar energy. A performance ratio of 15 was reported for this device.

A separate study (Muthunayagam et al., 2005) investigated the temperature shift in water drops during spraying. A vapor model was developed based on the results obtained. The outcomes of their research point out that the superheat temperature and the operational pressure are the most critical parameters affecting the spray process and system performance. It is essential to optimize these systems to establish optimal settings. To this extent, an optimization study (Ahmed et al., 2023) on the flashing-type desalination device was done using response surface methodology. An optimum distillate of 7010 ml/h was reported. Similarly, it was found that upward-traveling feed water resulted in better system performance in comparison to downward-traveling feed water (Ikegami et al., 2006). Nonetheless, a different study (Fathinia et al., 2019) reported that augmenting the flow rate enhances the system efficiency irrespective of fluid direction. However, the flash efficiency decreased with an increase in the flow rate. The impact of salinity (Ahmed et al., 2024) on flashing-type desalination systems was also investigated, and it was reported that the salinity has a negative effect on the distillate production. A review (Vaithilingam et al., 2021) was performed on different desalination systems that were combined with solar energy, considering the energy efficiency, exergy efficiency, and the economic factors. According to this review, desalination systems that use solar energy are more economical and efficient than those that use alternative energy sources. A new desalinating unit relying on solar and geothermal energy was examined in another investigation (Li et al., 2023). This system's energy efficiency was reported to be 22 %. In another study, a comparison of solar stills and flash evaporation systems was done. The output of flash evaporation systems was three times that of solar stills (Thakkar et al., 2022). In a similar vein, the impacts of solar-powered desalination systems on the environment were examined (Elsaid et al., 2020). This study revealed that the main elements impacting the environment are energy consumption, chemical reagents, exhaust emissions, brine disposal, and salt content of feed water. Nonetheless, it was found that the energy consumed and the brine disposition had a more significant overall impact on the environment. As a result, more studies in this direction were suggested to improve the environmental friendliness of such systems. A few other scientists (Gnaifaid and Ozcan, 2020) recently investigated whether concentrated solar power could be used simultaneously for electricity production and desalination. These scientists recommended that future research should focus on the concentration of solar energy in desalination devices to augment their efficiency and ensure sustainability. They also reported that adding thermal energy storage can enhance the system's performance. To this extent, in one recent study (Ahmed et al., 2024), process intensification of flashing-type desalination devices was carried out by employment of concentrated solar energy. Other techniques for enhancing efficiency include the use of photocatalysts (Pattnaik et al., 2023), nanofiltration technology (Samavati et al., 2023), protein crystallization (Mitchell et al., 2023), integration of renewable ammonia for sustainable energy (Palys et al., 2021), waste heat recovery and its integration with the primary process (Naeimi et al., 2020), employment of advanced oxidation techniques such as thermal activation of persulfates (Li et al., 2022), utilization of algorithms for system optimization (Yang et al., 2023), and dry powder coatings for minimizing energy losses (Khala et al., 2023).

Specific conditions could likely disrupt the incoming solar energy. In some cases, the amount of energy accessible through the sun might be inadequate. This condition results in a dip in the operating fluid temperature, which subsequently lowers system performance. This study introduces a unique concentrating solar-powered distillation device to address such difficulties. This concept is envisaged to foster additional advancement and enhancement of desalinating units. The setup proposed in this research employs a direct heating mechanism instead of the indirect heating method used in traditional systems. In addition, the system exhibits pressure alteration capability, which enables it to function effectively even in situations with little solar radiation. An innovative aspect of the suggested setup is the combination of multiplex characteristics: alteration of the flash compartment's pressure depending on the temperatures of brine to achieve distilled water even under challenging ambient circumstances, focusing solar irradiation onto a disc affixed to the brine heat exchanger to augment energy exchange and feed water heating through direct and concentrating solar irradiation by utilizing a parabolic concentrating unit. The impact of flow rate on three system outputs, namely, distillate production, condenser temperature, and brine heater temperature, is experimentally examined. Additionally, correlations are developed between various system responses and flow rates using Design Expert software. Currently, no such relationships are available in the literature on flash desalination systems. The energetic and exergetic performance of the flash vessel, brine heater, and condenser is evaluated. The proposed new configuration of the system is assessed by employing a variety of performance indices like specific energy consumption, energy utilization factor, and gain output ratio. This research is related to developments in process enhancement since it proposes an innovative desalination setup linked to concentrated solar power, enabling the device to maintain or increase the amount of distillate production while also reducing the size of the apparatus. Specifically, when employing concentrated solar energy instead of alternative methods, such as flat plate collectors, the area and size of the brine heat exchanger can be significantly decreased. Overall, this research presents a novel strategy to address issues with solar energy availability and proposes a unique desalination unit driven by concentrated solar energy that incorporates multiple features to excel in challenging circumstances.

2. Experimentation setup

The front and back views of the experimentation setup are exhibited in Fig. 1. This configuration incorporates a number of tanks, like the

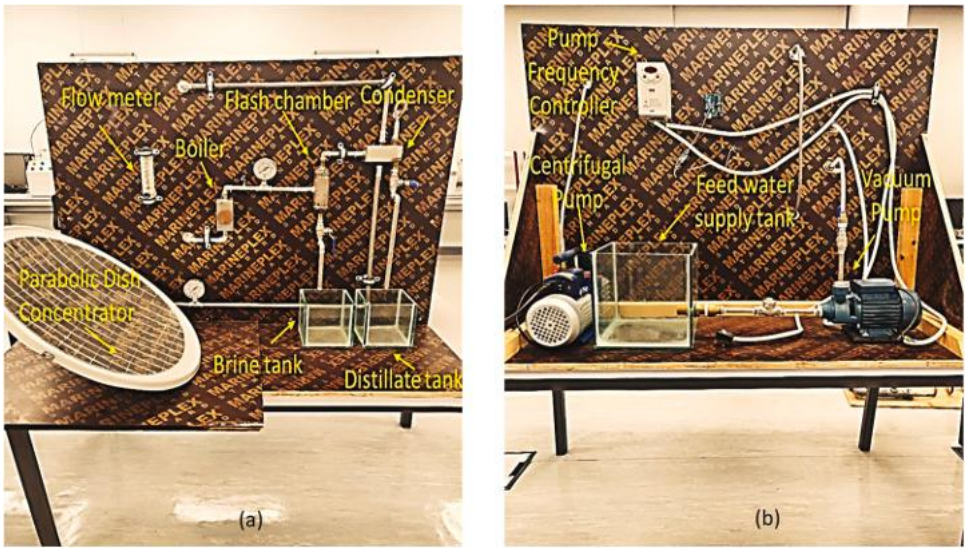

Fig. 1. Frontal view (a) and rear sight (b) of the experimental arrangement.

supply tank and distilled water collecting tank. The vacuum pump, concentrator plate, flow controller, centrifugal pump, brine heater, condenser, nozzle, flash chamber, and measuring sensors and gauges are some of the other parts. The complete setup was designed to be a tabletop device with geometrical constraints of 1.5 m as length, 0.5 m as breadth, and 1.5 m as height. Since a larger setup would lead to difficulties in the control and operation of the device, hence the experimental setup was designed to the specifications listed in Table 1. A hardwood baseboard supports the complete setup, and in order to prevent erosion, stainless steel was utilized in the construction of the brine heater, flashing vessel, connecting tubes, and condenser. All of the tanks were constructed with glass. Copper was used to fabricate the concentrator plate because of its strong heat conductivity. Reflecting mirrors on the steel parabolic dish will direct the incoming solar energy toward the absorbing material. The spacing between different parts is exhibited in Table 2, whereas the measurement capabilities and uncertainties of used instruments are detailed in Table 3.

Fig. 2 depicts the schematic and process representation for the experimentation unit. Initially, raw samples of feeding water were acquired from the shores of the eastern part of Saudi Arabia and analyzed. Experiments were carried out under the sun during the month of summer (June). A centrifugal pump transmits the feeding liquid forward to the condenser. The flow rate throughout the transport process is gauged by a flow meter, and a variable frequency motor controls the flow. Through heat exchange within the condenser, raw water enters at a lesser temperature and subsequently picks up the heat during its movement inside the condenser. The temperatures are recorded by virtue of the thermocouple sensor affixed next to the condenser's outflow region. Next, the feed water is sent to the brine heater, which is heated by incoming radiation on the absorber plate that acts as a solar energy concentrator. In this concentrating plate, solar energy is reflected by a parabolic dish and focused by its focal point. By passing through the brine heat exchanger, the raw water gains heat and exits the brine heater at a higher temperature. High-temperature water is blasted into the flashing container, causing flashes to be produced by pressure variations and the generation of vapors. Hot vapors condense inside the condenser region. The obtained pure water is collected separately. The concentrated brine from the flash vessel is disposed of in a brine disposal tank. By means of creating a pressure gradient in the condenser and flash unit, a vacuum pump provides a sucking action within the condenser to assist in the quicker movement of vapors between the two components. The vacuuming degree in the condenser is altered via a controlling lever affixed to the vacuuming pump. The technique and procedures of the experimentation are illustrated in Fig. 3. In this experiment, the vacuuming degree was kept at 0.5 bar, and the feed temperature was 50 °C.

Table 1
Parts and their specifications.

S. No	Part	Specification *(Length × Breadth × Height)*
1	Platform	1.5 × 0.5 × 1.5 m
2	Brine heater	0.05 × 0.05 × 0.1 m
3	Condenser	0.05 × 0.05 × 0.10 m
4	Flash chamber	0.1 × 0.1 × 0.2 m
5	Concentrator plate	Diameter = 0.05 m
6	Spray nozzle	0.002 m
7	Centrifugal pump	368 W
8	Hoses	0.006 m
9	Fluid tanks	0.005 m^3
10	Parabolic dish	Radius = 0.28 m

Table 2
Component spacing.

S. No	Component	Distance (m)
1	Condenser to distillate tank	0.4
2	Flash chamber to the brine tank	0.3
3	Brine heater to flash chamber	0.3
4	Flow meter to condenser	1.8
5	Feed pump to flow meter	0.3
6	Feeding tank to the feeding pump	0.35
7	Condenser to brine heater	1.3

Table 3
Instrument uncertainty.

S. No	Property	Tool	Measuring range	Uncertainty level
1	Flow rate	Flow meter	0.1 till 1.6 L/min	±1.25 %
2	Temperature	Thermocouples	-40 till 950 °C	±1.25 %
3	Solar radiation	Solar meter	200 till 1300 W/m^2	±1.5 %

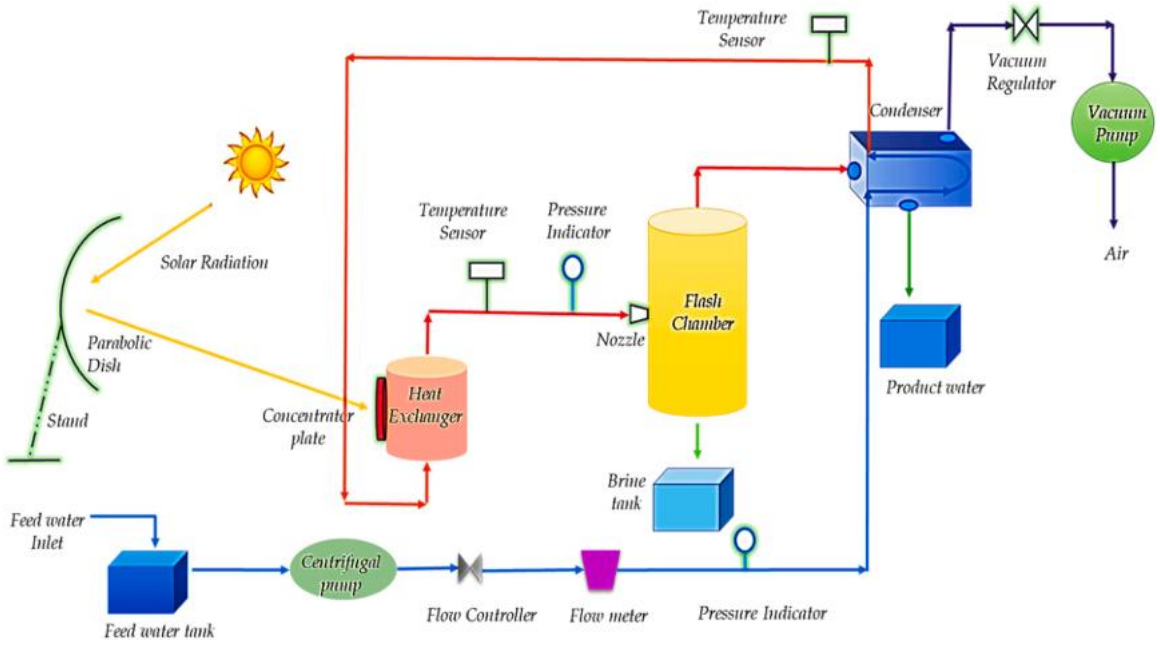

Fig. 2. Schematical representation of the experimentation facility.

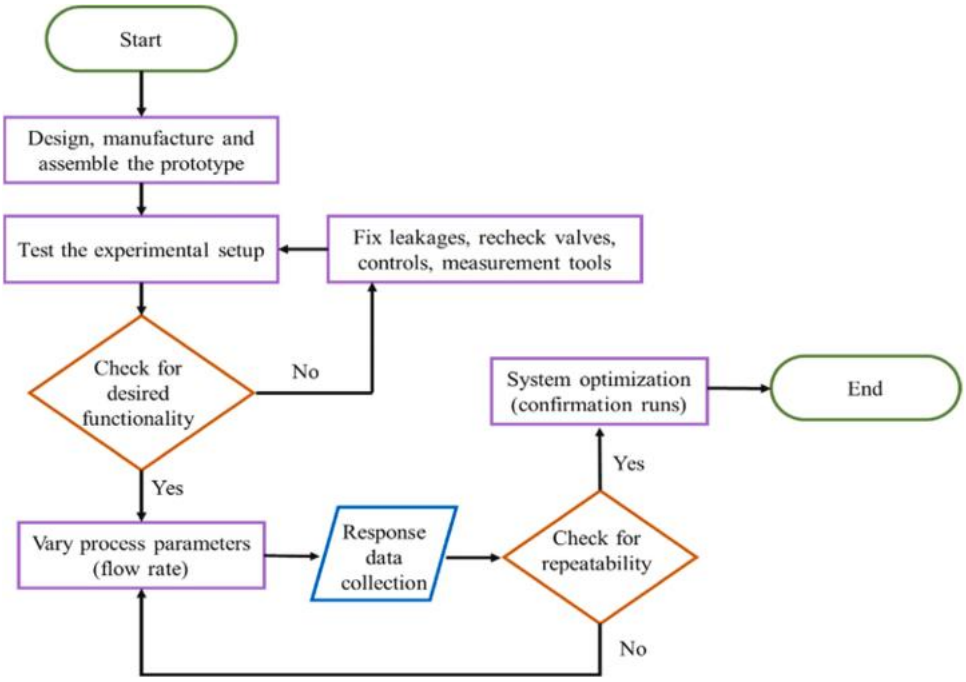

Fig. 3. Flowchart for the experimentation procedure.

3. Methods

3.1. Brine Heater's Energetic Analysis

Eqs. (1–8) are employed as per the analysis shown in a recent study (Malik et al., 2020). Eq. (1) calculates the heat transmitted to the feed supply.

$$Q_{abs} = \dot{m}_{fw} C_p (T_o - T_i) \tag{1}$$

where:

T_i represents inward temperatures, K

T_o represents outward temperatures, K

C_p represents heat capacity, J/kg K

Q_{abs} represents heat transmisison, W

$\dot{m}_{fw}$ represents flow rate, kg/s

The density of the supply water was taken as 1014 kg/m^3. Similarly, the specific heat of the supply water was taken as 4010 J/kgK, which again depends on the salt levels and temperature.

The brine heater experiences heat losses, and Eq. (2) is used to express this loss.

$$Q_L = U_L A (T_c - T_e) \tag{2}$$

where:

Q_L represents heat losses, W

T_e represents ambience temperature, K

A represents the exchanger area, m^2

T_c represents wall temperature, K

U_L represents losses coefficient, W/m^2 K

The area of heat transfer is a calculated value and is 0.028 m^2. The ambient temperature during the analysis was recorded as 35 °C.

The incoming renewable heat supply to the equipment is expressed by the relationship shown in Eq. (3).

$$Q_{in} = I_t(\tau\alpha)A \tag{3}$$

where:

I_t represents cumulative intensity, W/m^2

τα represents the coefficient of transmittivity-absorptivity

Q_{in} represents input energy, W

The heat absorption of feed water is estimated by Eq. (4).

$$Q_{abs} = I_t(\tau\alpha)A - U_L A(T_c - T_a) \tag{4}$$

A transmittance-absorptance coefficient of 0.9 was assumed, while the coefficient of heat loss was taken as 3 W/m^2K. Afterwards, calculations were done to estimate the total radiation.

The brine heat exchanger's energetic efficiency is estimated by means of Eq. (5).

$$\eta_{EN-EFF} = \frac{Q_{abs}}{Q_{in}} \tag{5}$$

3.2. Brine Heater's Exergetic Analysis

The exergetic destruction is computed by means of Eq. (6) and Eq. (7).

$$\dot{X_{des}} = \dot{X_T} - \dot{X_U} \tag{6}$$

$$\dot{X_{des}} = IA\left(1 - \frac{T_e}{T_s}\right) - \eta_{EN-CPHE}Q_{ab}\left(1 - \frac{T_e}{T_{fm}}\right) \tag{7}$$

where:

T_s represents the sun's temperature, K

T_{fm} represents the fluid's temperature, K

To determine the exergetic efficiency, Eq. (8) is utilized.

$$\eta_{EX-EFF} = \eta_{EN-CPHE}\left(\frac{\dot{X_U}}{\dot{X_T}}\right) \tag{8}$$

3.3. Flash Chamber's Energetic Analysis

The method introduced in recent research (Malik et al., 2020) is employed in conducting energy and exergy calculations for the flash chamber and is represented by Eqs. (9–24).

Eq. (9) describes the conservation of mass in the flash vessel.

$$\dot{m_f} = \dot{m_v} + \dot{m_b} \tag{9}$$

The flow rate of generated vapors can be computed as represented by Eq. (10).

$$\dot{m_v} = \dot{m_f}\frac{C_p(T_u - T_d)}{h_{fg}} \tag{10}$$

where:

T_u represents the feed's temperature (upstream conditions), K

T_d represents the feed's temperature (saturation, downstream conditions), K

$\dot{m_v}$ represents vapor flow, kg/s

h_{fg} represents enthalpy, kJ/kg

For vaporizing $\dot{m_v}$ kg of supply water, the needed heat is determined using Eq. (11).

$$\dot{Q_v} = \dot{m_v}h_{fg} \tag{11}$$

The above heat is taken from brine $\dot{m_b}$ and subsequently, Eq. (12) can be utilized for the computation of brine temperature.

$$\dot{Q_v} = \dot{m_b}C_p(T_u - T_b) \tag{12}$$

3.4. Flash Chamber's Exergetic Analysis

Eq. (13) describes the exergy balance of the flash vessel.

$$E_f = E_i - E_o - E_L \tag{13}$$

where:

E_i represents inward exergy of flashing vessel, kW

E_f represents flash chamber exergy, kW

E_L represents exergy losses, kW

E_o represents outward exergy of flashing vessel, kW

Eq. (14) describes the exergy loss, comprising three elements: diffusion, heat, and pressure.

$$E_L = E_{L,P} - E_{L,d} - E_{L,h} \tag{14}$$

where:

$E_{L,P}$ represents exergetic loss corresponding to pressure loss, kW

$E_{L,d}$ represents diffusion exergy loss, kW

$E_{L,h}$ represents exergetic losses corresponding to heat, kW

The losses of exergy by diffusion are generally regarded as non-significant. Thus, it is not taken into account in this analysis. Instead, the exergetic losses due to heat and drop in pressure are computed by means of Eq. (15) and Eq. (16).

$$E_{L,P} = \dot{m}_{fw}C_p\frac{T_e\Delta T^2}{2T_v(T_v + 0.5\Delta T)} \tag{15}$$

$$E_{L,h} = \dot{m}_{fw}C_pT_e\left[\ln\frac{T_v}{T_s} + \frac{T_s - T_v}{T_v}\right] \tag{16}$$

where:

T_v represents the temperature of vapor, K

ΔT represents the flashing vessel gradient temperature, K

Eq. (17) and Eq. (18) are employed for the determination of exergy of the flashing unit.

$$E_i = \dot{m}_i[(h_i - h_o) - T_o(S_i - S_o)] \tag{17}$$

$$E_o = \dot{m}_b[(h_b - h_o) - T_o(S_b - S_o)] \tag{18}$$

where:

h_i represents feed's enthalpy (inward to the vessel), kJ/kg

S_i represents feed's entropy (inward to vessel), kJ/kgK

h_b represents brine's enthalpy (outward from vessel), kJ/kg

S_b represents brine's entropy (outward from the chamber), kJ/kgK

The flash chamber's exergetic efficiency is written as shown in Eq. (19).

$$\eta_{EX-F} = \frac{E_f}{E_i} \tag{19}$$

3.5. Condenser's Energetic Analysis

Due to a brief contact period between the vapors and condenser, a high flow rate is necessary to condense the vapors effectively.

The heat transfer inside the condenser is estimated by means of Eq. (20).

$$\dot{Q} = \dot{m}_{cw}C_{p,cw}\left(T_{c,out} - T_{c,in}\right) \tag{20}$$

3.6. Condenser's Exergetic Analysis

Eq. (21) shows the representation of the condenser's exergy balance.

$$E_{ci} = E_{co} + E_{CL} \tag{21}$$

Exergetic losses in the condenser are estimated by means of Eq. (22).

$$E_{CL} = \dot{m}_{cw} T_e C_p \left[\ln \frac{T_{d2}}{T_{d1}} + \frac{T_{d1} - T_{d2}}{T_f} \right] \tag{22}$$

where:

T_{d1} represents the feed's entering temperature, K
T_f represents the distilled water temperature, K
T_{d2} represents the feed's exiting temperature, K

It is worth noting that the exergy going into the condenser equals the exergy of vapor generated in the flashing vessel. Thus, Eq. (23) and Eq. (24) are utilized to estimate the exergetic efficiency of the condenser.

$$E_c = E_f \tag{23}$$

$$\eta_{EX-C} = 1 - \frac{E_{CL}}{E_C} \tag{24}$$

3.7. Coefficient of Heat Transfer

A model developed by Jacimovic is employed here in Eqs. (25–29) to find the heat transfer coefficient (Jacimovic et al., 2018). The Nusselt number correlation is shown in Eq. (25).

$$Nu = Nu_{fd} + \frac{0.01 Gz^{1.7}}{1 + 0.001 Gz^{1.3}} \left(\frac{\mu}{\mu_w} \right)^{0.14} \tag{25}$$

where:

Nu_{fd} represents the fully developed flow value (taken to be 4.364)
μ_w represents the wall's viscosity, Pa.s
μ represents brine's viscosity, Pa.s
Gz represents Graetz number
Nu represents Nusselt number

The Graetz number is computed by means of Eq. (26).

$$Gz = \frac{D}{L} * \mathrm{Re} * \mathrm{Pr} \tag{26}$$

where:

Pr represents Prandtl number
Re represents Reynolds number
D represents the hydraulic diameter of brine heat exchanger, m
L represents the brine heater's longitudinal dimension, m

Eq. (27) is utilized to compute the Reynolds number.

$$\mathrm{Re} = \frac{\rho V D}{\mu} \tag{27}$$

where:

V represents feed velocity, m/s
ρ represents feed density, kg/m^3

Utilizing Eq. (28), the Prandtl number is estimated, which represents the momentum diffusivity of a fluid with respect to the thermal diffusivity.

$$\mathrm{Pr} = \frac{\mu * C_P}{k} \tag{28}$$

where:

k represents feed water conductivity, W/mK

Eq. (29) assists in the computation of the coefficient for heat transfer.

$$h = \frac{k * Nu}{D} \tag{29}$$

where:

h represents heat transfer coefficient, W/m^2.K

3.8. System's Evaporating Rate

During the flash desalination process, the quantity of water evaporated is called the evaporation rate. Eq. (30) assists in the computation of the evaporation rate (Araghi et al., 2017).

$$ER = \frac{\dot{m}_d}{\dot{m}_{fw}} \tag{30}$$

where:

$\dot{m}_d$ represents the flow of make-up water, L/min
ER represents the rate for evaporation of water

3.9. System's Output Ratio

This ratio (GOR) is an evaluation of the efficiency of a desalination unit. It is computed (Zheng, 2017) by means of Eq. (31).

$$GOR = \frac{\dot{m}_d h_{fg}}{Q_{in}} \tag{31}$$

where:

Q_{in} represents the thermal energy input, kW

Eq. (32) is employed to find the latent heat (Hamed et al., 2015).

$$h_{fg} = 2500.79 - 2.36418 * T + 0.00158927 * T^2 - 0.000061432 * T^3 \tag{32}$$

3.10. Proposed System's Specific Energy Consumption

Eq. (33) is utilized for calculating specific energy consumption (Lawal et al., 2018).

$$SEC = \frac{\dot{E}_{in}}{\dot{V}_d} \tag{33}$$

where:

$\dot{V}_d$ represents distilled water flow, m^3/h
$\dot{E}_{in}$ represents cumulative inward energy, kW
SEC represents the specific energy consumption, kWh/m^3

Eq. (34) describes the cumulative energy in the system (Lawal et al., 2018).

$$\dot{E}_{in} = \dot{W}_{feed} + \dot{W}_{vac} + \dot{Q}_{in} \tag{34}$$

where:

$\dot{W}_{vac}$ represents the vacuuming power, kW
$\dot{W}_{feed}$ represents the feeding power, kW

3.11. Proposed System's Utilization Factor

Desalination devices are also assessed by their energy utilization factor (EUF). Eq. (35) is employed (Chiranjeevi and Srinivas, 2015) to compute the energy utilization factor.

$$EUF = \frac{\dot{m}_d h_{fg}}{\dot{Q}_{in} + \dot{W}_{feed} + \dot{W}_{vacuum}} \tag{35}$$

4. Analysis of uncertainty

There are uncertainties in many different elements (ω_{M1}, ω_{M2},.... ω_{Mn}) that contribute to the uncertainties in the calculation of outcome (R). This uncertainty in the computed result is listed as follows (Sharqawy et al., 2009).

$$\omega_R = \left[\left(\frac{\delta R}{\delta M_1} \omega_{M_1} \right)^2 + \left(\frac{\delta R}{\delta M_2} \omega_{M_2} \right)^2 + \ldots + \left(\frac{\delta R}{\delta M_n} \omega_{M_n} \right)^2 \right]^{\frac{1}{2}} \quad (36)$$

where:

$M_1, M_2, \ldots M_n$ are factors, and R is the computed result. The uncertainty of individual parameters are ($\omega_{M1}, \omega_{M2}, \ldots \omega_{Mn}$). The uncertainties in any result can be estimated by means of Eq. (36). The uncertainties in *EUF, SEC, GOR,* $\eta_{EX\text{-}EFF}$, and $\eta_{EN\text{-}EFF}$ are computed by application of the above equation to each of the individual equations governing these parameters. Table 4 illustrates the computed uncertainties in these parameters.

5. Results and discussion

One of the crucial factors affecting flash desalination systems' performance is the flow rate (Alrowais et al., 2020). Our evaluation investigates the dependency of distillate with flow rate in flash desalination devices. A key component of optimizing distillate is evaluating how flow rate affects the overall process.

Fig. 4 depicts the quantity of heat transferred to the feed liquid. The heat gain of feed liquid is augmented, corresponding to augmentation in flow from 0.2 L/min onwards. For 0.6 L/min, there is a maximum heat transfer of 201.72 W to the feed water, while further incrementation in flow rate leads to a decline of heat transfer. This result indicates that the heat transfer varies as the flow rate varies. For flow rates greater than 0.6 L/min, the contact time for heat exchange between the feed water and the flashed vapors decreases, thus reducing the heat gained by feed water at higher flow rates. Further, based on the design of the apparatus, the available heat transfer area of the condenser also contributes to the sudden drop in the heat gain of feed water for flow rates greater than 0.6 L/min.

Using the methodology described in Section 3, the condenser's exergetic analysis was conducted. Fig. 5 exhibits the condenser's exergetic efficiency at different flow rates. Accordingly, the exergetic efficiency of the condenser does not vary as much as the flow rate. For all the tested flow rates, the average exergy efficiency was 89 %. For the highest tested flow rate of 1 L/min, a small jump in the exergy efficiency is observed. Considering the full range of tested flow rates, the exergy efficiency of the condenser was found to be high. This is attributed to many factors, such as the small size of the condenser, less heat transfer area between the flashed vapors and feed water, and the geometric configuration (shell with inner tube) of the condenser.

The energy efficiency of the brine heater is illustrated in Fig. 6, while the exergy efficiency is exhibited in Fig. 7, corresponding to various flow rates. The energy efficiency of the brine heater was found to augment with augmentation in flow rate from 0.2 L/min to 0.4 L/min. However, with a further increase in flow rate until 1 L/min, the energy efficiency was observed to decrease. For a flow rate of 0.4 L/min, an optimum energy efficiency of 40.6 % is achieved. At lower flow rates, the brine heater is observed to exhibit efficient heat transfer. The brine heater exhibited an average energy efficiency of 32 %, which corresponded to the tested flow rates. Similarly, a maximum exergy efficiency of 6.4 % is observed, corresponding to the flow rate of 0.4 L/min. The brine heater's average exergy efficiency was determined to be 4 %, which corresponds to the tested flow rates.

Table 4
Results and their uncertainty levels.

Factor	Uncertainty
Energy Utilization Factor (*EUF*)	4.1 %
Specific Energy Consumption (*SEC*)	2.76 %
Exergy efficiency ($\eta_{EX\text{-}EFF}$)	3.8 %
Gain Output Ratio (*GOR*)	3.6 %
Energy efficiency ($\eta_{EN\text{-}EFF}$)	3.38 %

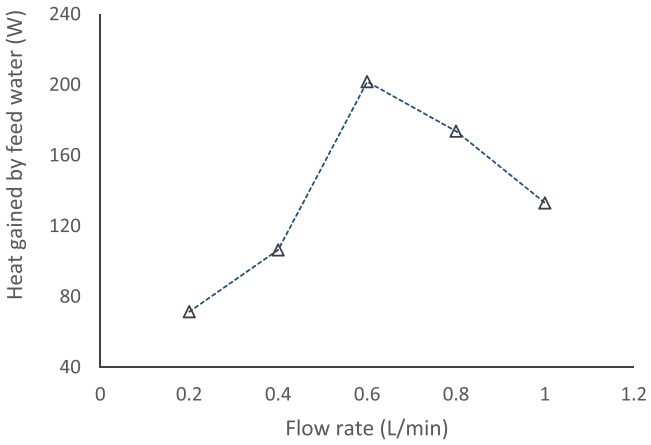

Fig. 4. Energy transfer in the condenser.

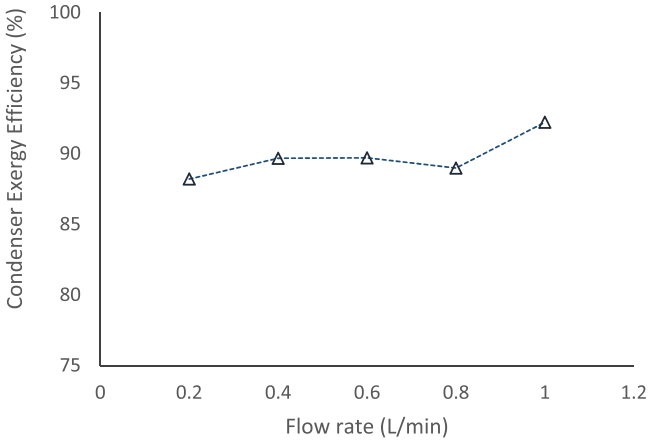

Fig. 5. Condenser's exergetic efficiency.

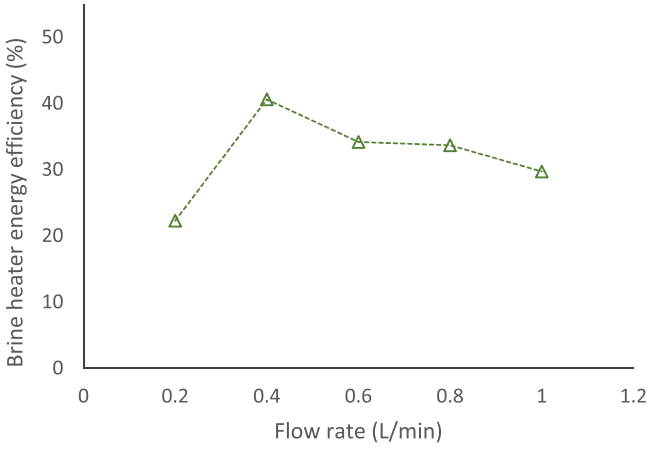

Fig. 6. Energy efficiency of brine heater.

Fig. 8 illustrates how the brine temperature altered with a change in flow rate. As can be seen, these brine temperatures decreased for higher flow rates. This is attributed to less heating of feed in the heater. This relatively less heated water flashes in the flash vessel, which leads to lower temperatures when departing the flashing unit. This brine exiting the flashing unit has an average exit temperature of 30.5 °C. Fig. 9 exhibits the exergetic performance of the flashing unit at a variety of flow rates. The energy efficiency of feed liquid is negatively affected by a rise

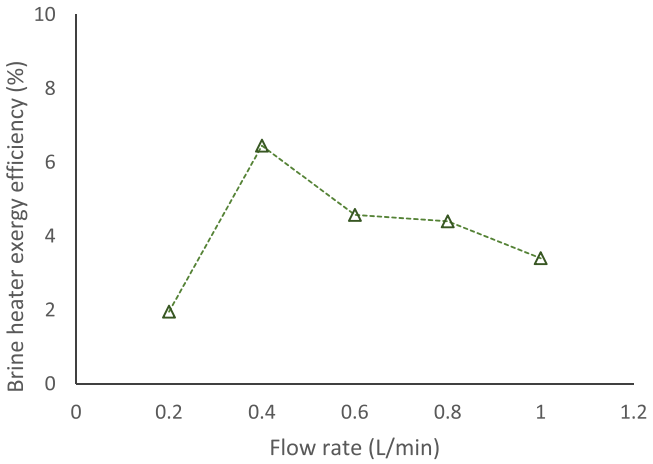

Fig. 7. Exergetic analysis of brine heater.

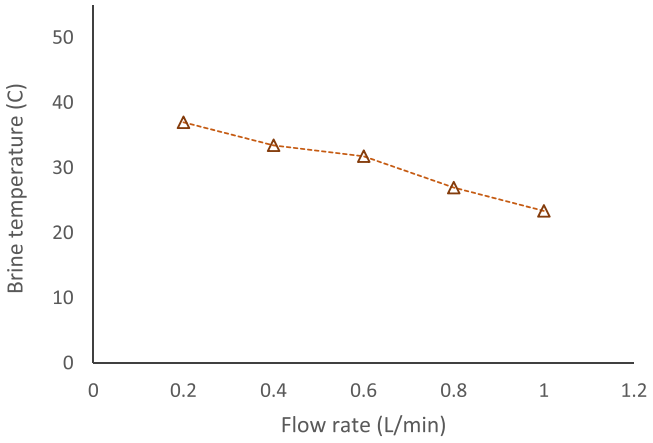

Fig. 8. Heat transfer across the flash chamber.

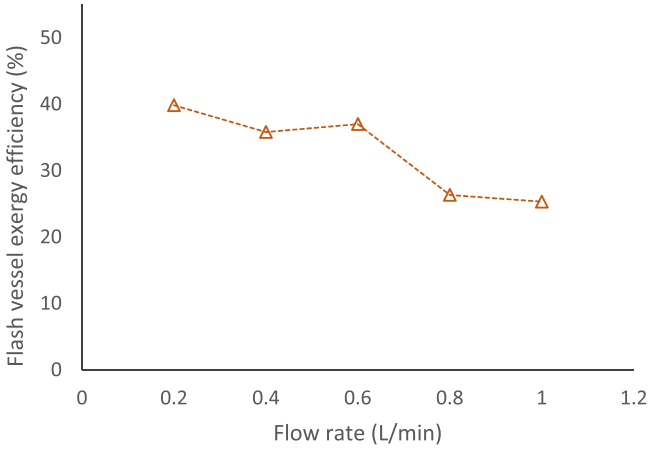

Fig. 9. Flash chamber's exergetic efficiency.

in flow rate. Also, the exergetic performance is reported to decline with an increased flow rate. The highest exergetic efficiency of 37 % is observed, corresponding to 0.6 L/min. An average exergetic efficiency of 32.8 % is reported for the range of flow rates tested.

Fig. 10 depicts the variation of distilled water corresponding to various flow conditions. The distillate was observed to rise with a rise in flow rate to 0.8 L/min. Further increase in flow rate leads to a drop in the volume of product water. The highest quantity of produced water is

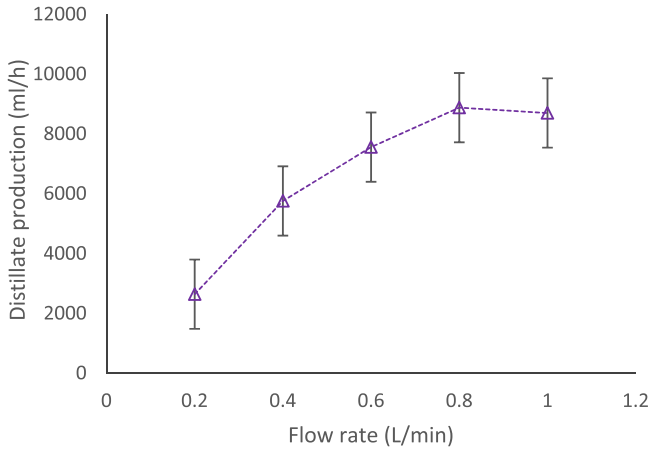

Fig. 10. Distillate production at various flow conditions.

8880 ml/h, corresponding to a flow of 0.8 L/min. Higher flow rates reduce residence time, while lower flow rates allow for increased residence time. The feed water's flow rate directly affects the water's residence time in the system. Residence time refers to the duration of water remains in the desalination chamber. At very high flow rates, the residence time decreases, and the water may not have sufficient time to fully vaporize before exiting the chamber. This can result in reduced distillate production as some water exits the system without being completely converted into vapor. Alternately, at very low flow rates, the residence time increases, which can lead to water overheating. Excessive residence time can cause thermal degradation of the distillate quality. It may also result in scaling problems inside the desalination device. Therefore, finding an optimal flow rate is crucial for maximizing distillation in flashing-type desalination devices. The optimal flow rate balances the residence time required for efficient vaporization and the throughput needed to maintain high productivity. However, it is critical to observe that the relation between flow rate and distillate production is not linear, as an optimal flow rate is specific to each system. Other parameters such as operating pressure, feed temperature, heat transfer efficiency, and proper design and operation of the equipment also have a crucial role in determining the device's overall performance. Hence, it is essential to consider these factors holistically while evaluating the impact of flow rate on distillate production.

Efficient heat transfer is necessary for optimal vaporization and subsequent condensation. Higher flow rates can decrease the contact time between the heated surfaces and the feedwater, reducing the overall heat transfer. This reduction in heat transfer can negatively impact distillate production. Increasing the flow rate can cause a higher pressure drop across the system, affecting the stability and performance of the flash desalination process. Several considerations should be considered when determining the flow rate to optimize distillate production in flash desalination systems. The flash chamber, brine heater, and condenser design should be well-matched to handle the desired flow rate. Adequate surface area for heat transfer and appropriate residence time must be ensured to enhance distillate production. Higher flow rates generally need more energy to maintain the required temperatures and pressures. Balancing the flow rate with energy consumption is crucial for achieving the required amount of distillated water.

The system's coefficient of heat transfer is plotted in Fig. 11 at various Reynolds numbers. At 1 L/min, a maximum heat transfer coefficient was obtained and is reported to be 3897.9 W/m^{2}K. The average coefficient of heat transfer is reported to be 3063.9 W/m^{2}K. The coefficient of heat transfer rose with incrementation in flow rate. Therefore, it is noted that the novel system exhibits a greater coefficient of heat transfer under turbulent flow conditions.

The evaporation rate is depicted in Fig. 12. The highest evaporation rate is determined to be 24 % for 0.4 L/min. The average evaporation

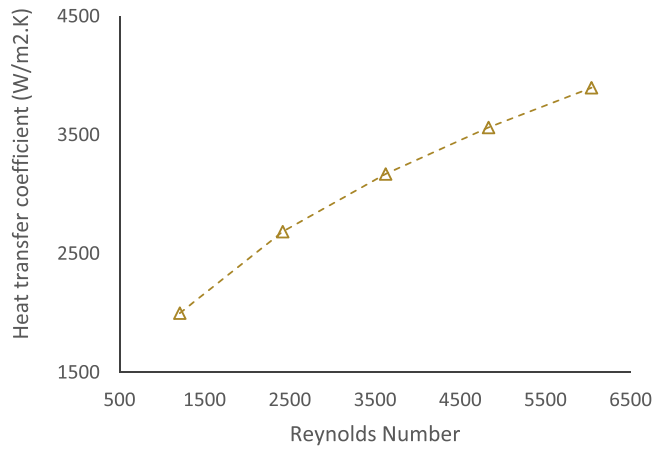

Fig. 11. Coefficient of heat transfer.

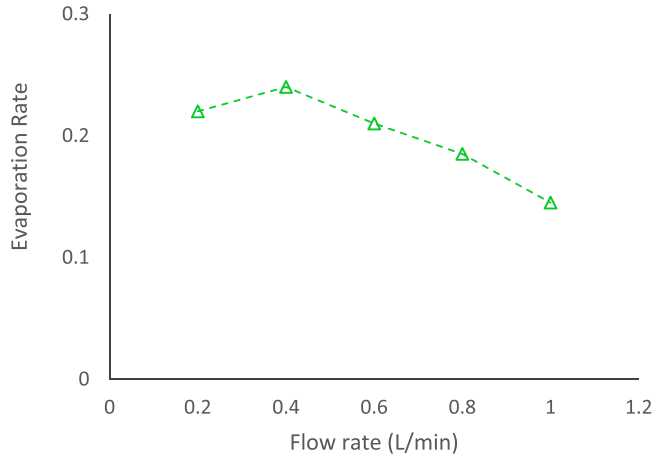

Fig. 12. Variation of evaporation rate.

rate is calculated to be 20 %. It is seen that although the rate of evaporation increased initially, it later declined continuously for all the tested flow conditions. This is attributed to lesser evaporation taking place at higher flow rates. Henceforth, it is appropriate to report that the flow rate in the proposed system negatively influences the vaporization. The proposed system exhibited higher evaporation rates in laminar flow conditions.

As illustrated in Fig. 13, the novel system exhibited the highest ratio of 15.5 at 0.8 L/min. A mean gain output ratio of 11.7 was achieved. The gain output ratio was found to augment starting with 0.2 L/min till 0.8 L/min, after which a slight decrease in gain output ratio occurred at the flow of 1 L/min. Therefore, the output ratio of the novel unit is found to be directly and positively influenced by the flow rate. The proposed system exhibited higher gain output ratios in turbulent flow conditions.

Fig. 14 exhibits the energy consumption of the proposed system for different flow patterns. The lowest energy consumed is reported to be 100.8 kWh/m^3 at 0.8 L/min, whereas the highest energy consumption was 339 kWh/m^3 at 0.2 L/min. According to the results of this study, 163.3 kWh/m^3 is the average energy requirement of this apparatus. When the flow was incremented, the specific energy consumption declined. Therefore, it is concluded that higher flow rates lead to reduced energy consumption for the novel unit. For turbulent flow conditions, the proposed system consumes less energy. The average energy consumption observed here is considered a reasonable level of energy consumption. Table 5 presents the competitiveness of the energy consumption of this novel device.

The variation of the energy utilization factor is exhibited in Fig. 15. At 0.2 L/min, the lowest energy utilization factor of 1.4 was found, while at 0.8 L/min, the highest energy utilization factor of 4.8 was found. Based on these results, an average energy utilization factor of 3.62 is reported for the proposed device. In this study, the energy utilization factor augmented with incrementation starting at 0.2 L /min till 0.8 L /min and then decreased slightly afterward. As a result, the proposed system exhibited a higher energy utilization factor for turbulent flow conditions, indicating that the flow rate is directly proportional to the energy utilization factor. While this device exhibits optimal performance at higher flow rates, the average energy utilization factor is regarded as a reasonable level of energy utilization. According to this study, the device is energy efficient and assists towards the advancement and integration of sustainable energy into desalination devices.

Fig. 16 exhibits the performance ratio of the proposed system. A comparison was established between the proposed device and other similar configured devices (Wessley and Mathews, 2015). The application of traditional collectors (Siddique et al., 2018) in desalinating units was the subject of earlier studies (Maroo and Goswami, 2009). In the current study, using concentrated solar energy resulted in a significant augmentation in the performance ratio. The ratio was found to reach 4.8. Furthermore, by utilizing concentrated solar power, this novel system outperforms earlier flat plate collector-based systems in terms of performance, indicating the possibility for more effective and sustainable desalination procedures.

Furthermore, in this study, mathematical equations are established using Design Expert software to express the relation between flow rate

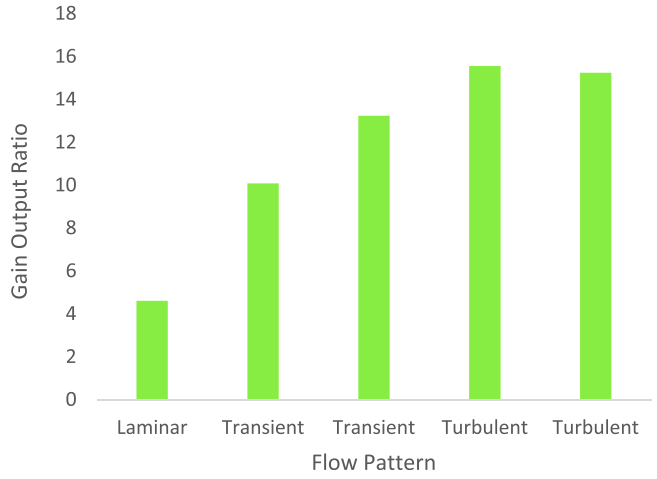

Fig. 13. Proposed system's gain output ratio.

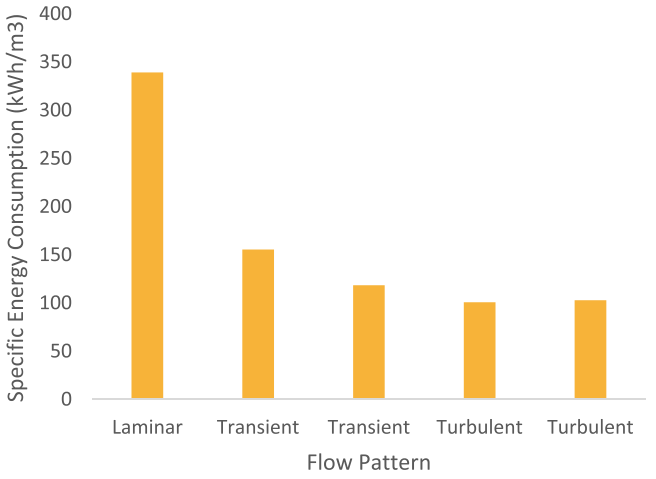

Fig. 14. Proposed system's specific energy consumption.

Table 5
Competitiveness of the proposed device.

Metric	Traditional flashing desalination unit	Flashing desalination unit-solar-based (Darawsheh et al., 2019)	Flashing system proposed in this research
Energy consumed (kWh/m^3)	94.4	567.2	100.8

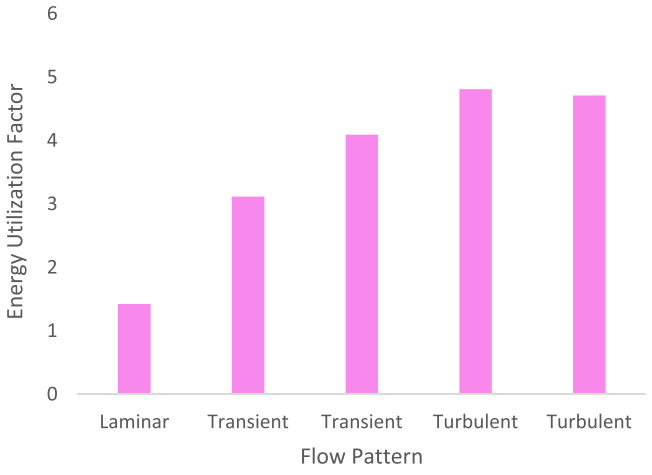

Fig. 15. Proposed system's energy utilization factor.

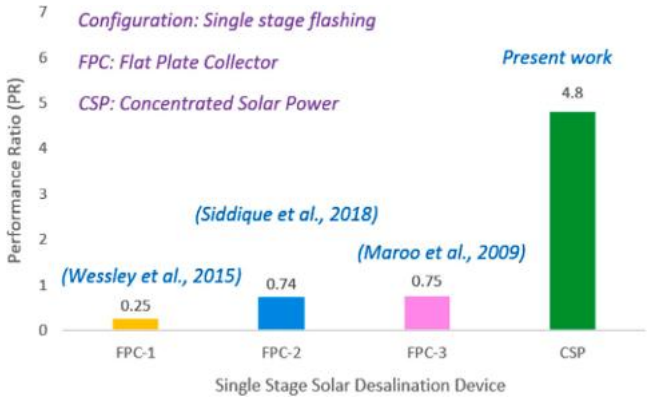

Fig. 16. Comparative analysis of the novel device.

and system responses. As described by Eqs. (37), (38) and (39), the flow rate is represented by the letter A, and hence the system responses can be predicted based on these equations.

$$\text{Condenser temperature} = +55.6 - (16.4)*(A) + (20.9)*(A^2) - (9.3)*(A^3) \quad (37)$$

$$\textit{Brine heater temperature} = +60.8 - (6.7)*(A) \quad (38)$$

$$\textit{Distillate} = -1404 + (22791.4)*(A) - (12642.8)*(A^2) \quad (39)$$

A cubical model resulted in the best fit with the experimental data for condenser temperature. Model-generated values and real-time condenser results are shown in Fig. 17. For this cubical model, the standard deviation was 0.012. Further, the value of R^2 was found to be 0.99. On the other hand, the best R^2 value for the brine heater is reported for a linear model. Fig. 18 exhibits the model-generated results and real-time results for the brine heater. For this linear model, the standard deviation was 0.47. Further, the value of R^2 is found to be 0.9. A quadratic model produced the best R^2 value in the distillate production scenario. The data produced from the model and the real-time distillation values are exhibited in Fig. 19. For this quadratic model, the

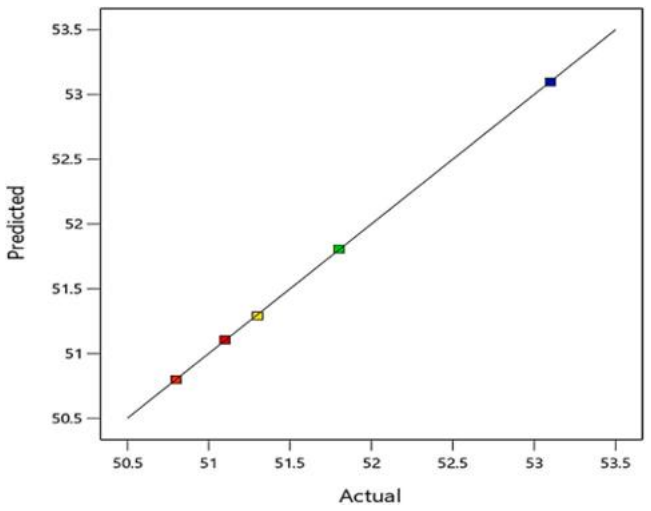

Fig. 17. Condenser temperature as per developed model.

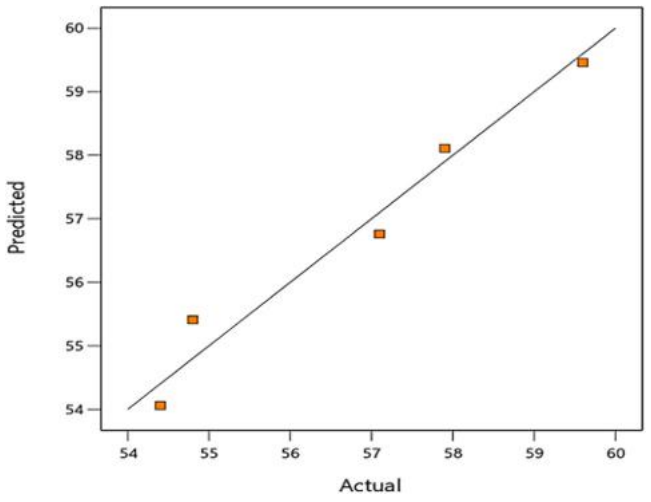

Fig. 18. Brine heater temperature as per developed model.

standard deviation is 162.27. The R^2 value is found to be 0.97.

For any desalination system to be effective and sustainable, routine maintenance and operational care will be needed. The anticipated lifespan of the proposed desalination device is 20–30 years. System sizing, the acquisition procedure, and other finance-related conditions influence this lifespan. Less than 20 % of the overall cost is devoted to operation and maintenance charges (Kabeel et al., 2019). The planned system's regular operation and maintenance expenses are listed in Table 6. Less carbon footprints and more environmentally friendly desalination are two key benefits of the proposed technology.

6. Conclusion

The main conclusions and findings from this research are listed below.

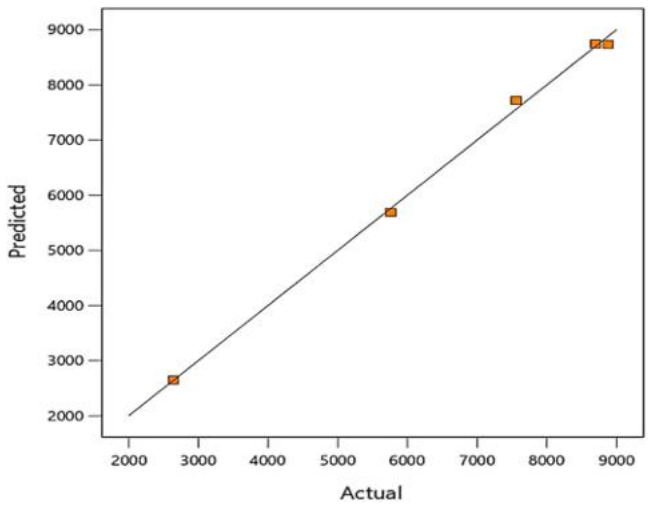

Fig. 19. Distillation as per developed model.

Table 6
Maintenance and operation expenses.

Expense	Factor	Percentage contribution towards the total expenses
Maintenance	Associated cleaning	6 %
	Minor device replacements	
	Pipelines	
	Pumps	
	Instruments	
Legal/ permitting	Permit compliances	2 %
	Environmental monitoring	
Operational	Chemicals	6 %
	Power (energy)	60 %
	Brine disposal	4 %
	Labour	12 %
	Other related	10 %

- This study revealed that distillation rises with an augmentation in the flow rate to an optimal level.
- An optimum distillation rate of 8880 ml/h can be achieved at 0.8 L/min for the tested range of flow rates.
- The mean energy efficiency of the brine heater was found to be 32 %.
- The mean exergy efficiencies of the brine heater, condenser and flashing chamber were 4.1 %, 89.2 % and 32.8 %, respectively.
- The proposed system has a maximum gain output ratio of 15.5, a maximum energy utilization factor of 4.8, and a minimum specific energy consumption of 100.8 kWh/m^3.

CRediT authorship contribution statement

Faizan Ahmed: Writing – original draft, Visualization, Validation, Software, Methodology, Investigation, Formal analysis, Conceptualization. **C.Y. Khor:** Writing – review & editing, Visualization, Software, Methodology. **Feroz Shaik:** Writing – review & editing, Supervision, Software, Investigation. **Mohd Sharizal Abdul Aziz:** Writing – review & editing, Validation, Supervision, Software, Investigation, Formal analysis, Conceptualization.

Declaration of Competing Interest

The authors declare that they have no known competing financial interests or personal relationships that could have appeared to influence the work reported in this paper.

Data availability

Data is available by placing a request to the corresponding author.

Acknowledgment

This work is financially supported by the Ministry of Higher Education (MOHE) Malaysia under the Fundamental Research Grant Scheme, FRGS (Grant number FRGS/1/2023/TK10/USM/02/5). The authors are grateful to Universiti Sains Malaysia for providing technical support.

References

Ahmed, F., Aziz, M.S., Palaniandy, P., Shaik, F., 2022. A review on application of renewable energy for desalination technologies with emphasis on concentrated solar power. Sustain. Energy Technol. Assess. 53, 102772 https://doi.org/10.1016/j.seta.2022. 102772.

Ahmed, F., Aziz, M.S., Shaik, F., Khor, C.Y., 2023. Optimization of a novel spray flash desalination system integrated with concentrated solar power utilizing response surface methodology. Desalination 558, 116640. https://doi.org/10.1016/j.desal.2023.116640.

Ahmed, F., Aziz, M.S., Shaik, F., Khor, C.Y., 2024. Performance assessment of a unique solar desalination device operating with concentrating solar power technology and variable feed temperatures. Chem. Eng. Process. -Process. Intensif., 109722 https://doi.org/10.1016/j.cep.2024.109722.

Alrowais, R., Qian, C., Burhan, M., Ybyraiymkul, D., Shahzad, M.W., Ng, K.C., 2020. A greener seawater desalination method by direct-contact spray evaporation and condensation (DCSEC): Experiments. Appl. Therm. Eng. 179, 115629 https://doi.org/10.1016/j.applthermaleng.2020.115629.

Araghi, A.H., Khiadani, M., Sadafi, M.H., Hooman, K., 2017. A numerical model and experimental verification for analyzing a new vacuum spray flash desalinator utilizing low grade energy. Desalination 413, 109–118. https://doi.org/10.1016/j.desal.2017.03.014.

Barba, D., Capocelli, M., 2023. Process analysis of the novel Flash-ME desalination process driven by low-grade thermal energy. Chem. Eng. Res. Des. 189, 721–733. https://doi.org/10.1016/j.cherd.2022.11.052.

Chen, L.X., Hu, P., Sheng, C.C., Zhang, N., Xie, M.N., Wang, F.X., 2019. Thermodynamic analysis of three ejector based organic flash cycles for low grade waste heat recovery. Energy Convers. Manag. 185, 384–395. https://doi.org/10.1016/j.enconman.2019.02.016.

Chiranjeevi, C., Srinivas, T., 2015. Experimental and simulation studies on two stage humidification–dehumidification desalination and cooling plant. Desalination 376, 9–16. https://doi.org/10.1016/j.desal.2015.08.006.

Darawsheh, I., Islam, M.D., Banat, F., 2019. Experimental characterization of a solar powered MSF desalination process performance. Therm. Sci. Eng. Prog. 10, 154–162. https://doi.org/10.1016/j.tsep.2019.01.018.

Dong, C., He, R., Xu, S., He, H., Chen, H., Zhang, Y.B., He, T., 2022. Layer-by-layer (LBL) hollow fiber nanofiltration membranes for seawater treatment: ion rejection. Desalination 534, 115793. https://doi.org/10.1016/j.desal.2022.115793.

Elsaid, K., Sayed, E.T., Abdelkareem, M.A., Mahmoud, M.S., Ramadan, M., Olabi, A.G., 2020. Environmental impact of emerging desalination technologies: a preliminary evaluation. J. Environ. Chem. Eng. 8, 104099 https://doi.org/10.1016/ j.jece.2020.104099.

Fathinia, F., Al-Abdeli, Y.M., Khiadani, M., 2019. Evaporation rates and temperature distributions in fine droplet flash evaporation sprays. Int. J. Therm. Sci. 145, 106037 https://doi.org/10.1016/j.ijthermalsci.2019.106037.

Gandhidasan, P., 2005. Quick performance prediction of liquid desiccant regeneration in a packed bed. Sol. Energy 79 (1), 47–55. https://doi.org/10.1016/j.solener.2004.10.002.

Gao, W., Qi, J., Zhang, J., Chen, G., Wu, D., 2019. An experimental study on explosive boiling of superheated droplets in vacuum spray flash evaporation. Int. J. Heat. Mass Transf. 144, 118552 https://doi.org/10.1016/j.ijheatmasstransfer.2019.118552.

Gnaifaid, H., Ozcan, H., 2020. Multi-objective optimization of a concentrated solar energy driven trigeneration plant with thermal energy storage: A case study for Turkey. Case Stud. Therm. Eng. 20, 100642 https://doi.org/10.1016/j.csite.2020.100642.

Hamed, M.H., Kabeel, A.E., Omara, Z.M., Sharshir, S.W., 2015. Mathematical and experimental investigation of a solar humidification–dehumidification desalination unit. Desalination 358, 9–17. https://doi.org/10.1016/j.desal.2014.12.005.

Ibrahim, I., Seo, D.H., McDonagh, A.M., Shon, H.K., Tijing, L., 2021. Semiconductor photothermal materials enabling efficient solar steam generation toward desalination and wastewater treatment. Desalination 500, 114853. https://doi.org/10.1016/j.desal.2020.114853.

Ikegami, Y., Sasaki, H., Gouda, T., Uehara, H., 2006. Experimental study on a spray flash desalination (influence of the direction of injection). Desalination 194 (1-3), 81–89. https://doi.org/10.1016/j.desal.2005.10.026.

Jacimovic, B., Genic, S., Lelea, D., 2018. Calculation of the heat transfer coefficient for laminar flow in pipes in practical engineering applications. Heat. Transf. Eng. 39 (20), 1790–1796. https://doi.org/10.1080/01457632.2017.1388949.

Ji, C., Cheng, L., Wang, N., Liu, Z., 2019. Experimental investigation on high-pressure high-temperature spray flash evaporation and the characteristic Jakob number. Exp.

Therm. Fluid Sci. 102, 94–100. https://doi.org/10.1016/j.expthermflusci.2018.10.018.
Kabeel, A.E., El-Said, E.M.S., Dafea, S.A., 2019. Design considerations and their effects on the operation and maintenance cost in solar-powered desalination plants. Heat. Transf. Asian Res. 48, 1722–1736. https://doi.org/10.1002/htj.21454.
Kaheal, M.M., Chiasson, A., Alsehli, M., 2023. Component-based, dynamic simulation of a novel once through multistage flash (MSF-OT) solar thermal desalination plant. Desalination 548, 116290. https://doi.org/10.1016/j.desal.2022.116290.
Khala, M.J., Hare, C., Karde, V., Heng, J.Y., 2023. A numerical analysis of the influence of material properties on dry powder coating performance. Chem. Eng. Res. Des. 193, 158–167. https://doi.org/10.1016/j.cherd.2023.03.028.
Lai, X., Long, R., Liu, Z., Liu, W., 2021. Solar energy powered high-recovery reverse osmosis for synchronous seawater desalination and energy storage. Energy Convers. Manag. 228, 113665 https://doi.org/10.1016/j.enconman.2020.113665.
Lawal, D.U., Zubair, S.M., Antar, M.A., 2018. Exergo-economic analysis of humidification-dehumidification (HDH) desalination systems driven by heat pump (HP). Desalination 443, 11–25. https://doi.org/10.1016/j.desal.2018.05.011.
Li, N., Wu, S., Dai, H., Cheng, Z., Peng, W., Yan, B., Chen, G., Wang, S., Duan, X., 2022. Thermal activation of persulfates for organic wastewater purification: heating modes, mechanism and influencing factors. Chem. Eng. J. 450, 137976 https://doi.org/10.1016/j.cej.2022.137976.
Li, R., Xu, D., Tian, H., Zhu, Y., 2023. Multi-objective study and optimization of a solar-boosted geothermal flash cycle integrated into an innovative combined power and desalinated water production process: application of a case study. Energy 282, 128706 https://doi.org/10.1016/ j.energy.2023.128706.
Malik, A., Qureshi, S.R., Abbas, N., Zaidi, A.A., 2020. Energy and exergy analyses of a solar desalination plant for Karachi Pakistan. Sustain. Energy Technol. Assess. 37, 100596 https://doi.org/10.1016/j.seta.2019.100596.
Maroo, S.C., Goswami, D.Y., 2009. Theoretical analysis of a single-stage and two-stage solar driven flash desalination system based on passive vacuum generation. Desalination 249, 635–646. https://doi.org/10.1016/j.desal.2008.12.055.
Mitchell, H.M., Jovannus, D., Rosbottom, I., Link, F.J., Mitchell, N.A., Heng, J.Y., 2023. Process modelling of protein crystallization: a case study of lysozyme. Chem. Eng. Res. Des. 192, 268–279. https://doi.org/10.1016/j.cherd.2023.02.016.
Miyatake, O., Koito, Y., Tagawa, K., Maruta, Y., 2001. Transient characteristics and performance of a novel desalination system based on heat storage and spray flashing. Desalination 137 (1-3), 157–166. https://doi.org/10.1016/S0011-9164(01)00214-4.
Muthunayagam, A.E., Ramamurthi, K., Paden, J.R., 2005. Low temperature flash vaporization for desalination. Desalination 180 (1-3), 25–32 https://doi.org/10.1016/ j.desal.2004. 12.028.
Naeimi, A., Nowee, S.M., Amiri, H.A., 2020. Numerical simulation and theoretical investigation of a multi-cycle dual-evaporator adsorption desalination and cooling system. Chem. Eng. Res. Des. 156, 402–413. https://doi.org/10.1016/j.cherd.2020.02.016.
Palys, M.J., Wang, H., Zhang, Q., Daoutidis, P., 2021. Renewable ammonia for sustainable energy and agriculture: vision and systems engineering opportunities. Curr. Opin. Chem. Eng. 31, 100667 https://doi.org/10.1016/j.coche.2020.100667.
Pattnaik, A., Sahu, J.N., Poonia, A.K., Ghosh, P., 2023. Current perspective of nano-engineered metal oxide based photocatalysts in advanced oxidation processes for degradation of organic pollutants in wastewater. Chem. Eng. Res. Des. 190, 667–686. https://doi.org/10.1016/j.cherd.2023.01.014.
Risse, B., Spitzer, D., Hassler, D., Schnell, F., Comet, M., Pichot, V., Muhr, H., 2012. Continuous formation of submicron energetic particles by the flash-evaporation technique. Chem. Eng. J. 203, 158–165. https://doi.org/10.1016/j.cej.2012.07.032.
Samavati, Z., Samavati, A., Goh, P.S., Ismail, A.F., Abdullah, M.S., 2023. A comprehensive review of recent advances in nanofiltration membranes for heavy metal removal from wastewater. Chem. Eng. Res. Des. 189, 530–571 https://doi.org/10.1016/j.cherd. 2022.11.042.
Sharqawy, M.H., Mokheimer, E.M., Habib, M.A., Badr, H.M., Said, S.A., Al-Shayea, N.A., 2009. Energy, exergy and uncertainty analyses of the thermal response test for a ground heat exchanger. Int. J. Energy Res. 33, 582–592. https://doi.org/10.1002/er.1496.
Siddique M., Turkmen N., Al-Rabghi O.M., Shabana E., Albeirutty M.H. Small-scale low pressure 'single effect distillation' and 'single stage flash' solar driven barometric desalination units: A comparative analysis. Desalination 2018; 444: 53-62. https://doi.org/10.1016/j.desal. 2018.06.011.
Tareemi, A.A., Sharshir, S.W., 2023. A state-of-art overview of multi-stage flash desalination and water treatment: principles, challenges, and heat recovery in hybrid systems. Sol. Energy 266, 112157. https://doi.org/10.1016/j.solener.2023.112157.
Thakkar, H., Sadasivuni, K.K., Ramana, P.V., Panchal, H., Suresh, M., Israr, M., Elklawy, M., AlmElDin, H., 2022. Comparative analysis of the use of flash evaporator and solar still with a solar desalination system. Int. J. Ambient Energy 43, 1561–1568. https://doi.org/10.1080/01430750.2020.1712242.
Vaithilingam, S., Gopal, S.T., Srinivasan, S.K., Manokar, A.M., Sathyamurthy, R., Esakkimuthu, G.S., Kumar, R., Sharifpur, M., 2021. An extensive review on thermodynamic aspect based solar desalination techniques. J. Therm. Anal. Calorim. 145, 1103–1119. https://doi.org/10.1007/s10973-020-10269-x.
Wessley, J.J., Mathews, K., 2015. Thermodynamic analysis of a single and two-stage solar assisted air-cooled flash evaporation desalination system for small-scale applications. Desalin. Water Treat. 54, 2364–2375. https://doi.org/10.1080/19443994.2014.901188.
Yang, A., Kong, Z.Y., Sunarso, J., 2023. Design and optimization of novel hybrid side-stream reactive-extractive distillation for recovery of isopropyl alcohol and ethyl acetate from wastewater. Chem. Eng. J. 451, 138563 https://doi.org/10.1016/j.cej.2022.138563.
Zheng, H., 2017. Fundamental relationships of heat and mass transfer in solar seawater desalination systems. Sol. Energy Desalin. Technol. 173–258. https://doi.org/10.1016/B978-0-12-805411-6.00003-8.